Octave-spanning coherent mid-IR generation via adiabatic difference frequency conversion

Haim Suchowski,[1] Peter R. Krogen,[2] Shu-Wei Huang,[2] Franz X. Kärtner,[2,3] and Jeffrey Moses[2]

[1]*NSF Nanoscale Science and Engineering Center, University of California, Berkeley, California 94720, USA*
[2]*Department of Electrical Engineering and Computer Science and Research Laboratory of Electronics, Massachusetts Institute of Technology, Cambridge, Massachusetts 02139, USA*
[3]*Center for Free-Electron Laser Science, DESY and Physics Department University of Hamburg, Notkestraße 85, D-22607 Hamburg, Germany*
*j_moses@mit.edu

Abstract: We demonstrate efficient downconversion of a near-IR broadband optical parametric chirped pulse amplifier (OPCPA) pulse to a 1.1-octave-spanning mid-IR pulse (measured at −10 dB of peak) via a single nonlinearly and adiabatically chirped quasi-phase-matching grating in magnesium oxide doped lithium niobate. We report a spectrum spanning from 2 to 5 μm and obtained by near full photon number conversion of μJ-energy OPCPA pulses spanning 680-870 nm mixed with a narrowband 1047-nm pulse. The conversion process is shown to be robust for various input broadband OPA pulses and suitable for post-amplification conversion for many near-IR systems.

OCIS codes: (320.7110) Ultrafast nonlinear optics; (320.6629) Supercontinuum generation.

References and links

1. P. Hamm and M. T. Zanni, *Concepts and Methods of 2d infrared Spectroscopy* (Cambridge University Press, 2011).
2. P. Colosimo, G. Doumy, C. I. Blaga, J. Wheeler, C. Hauri, F. Catoire, J. Tate, R. Chirla, A. M. March, G. G. Paulus, H. G. Muller, P. Agostini, and L. F. DiMauro, "Scaling strong-field interactions towards the classical limit," Nat. Phys. **4**(5), 386–389 (2008).
3. D. Brida, M. Marangoni, C. Manzoni, S. D. Silvestri, and G. Cerullo, "Two-optical-cycle pulses in the mid-infrared from an optical parametric amplifier," Opt. Lett. **33**(24), 2901–2903 (2008).
4. N. Leindecker, A. Marandi, R. L. Byer, K. L. Vodopyanov, J. Jiang, I. Hartl, M. Fermann, and P. G. Schunemann, "Octave-spanning ultrafast OPO with 2.6-6.1 μm instantaneous bandwidth pumped by femtosecond Tm-fiber laser," Opt. Express **20**(7), 7046–7053 (2012).
5. C. Erny, K. Moutzouris, J. Biegert, D. Kühlke, F. Adler, A. Leitenstorfer, and U. Keller, "Mid-infrared difference-frequency generation of ultrashort pulses tunable between 3.2 and 4.8 μm from a compact fiber source," Opt. Lett. **32**(9), 1138–1140 (2007).
6. A. Sell, R. Scheu, A. Leitenstorfer, and R. Huber, "Field-resolved detection of phase-locked infrared transients from a compact Er:fiber system tunable between 55 and 107 THz," Appl. Phys. Lett. **93**(25), 251107 (2008).
7. Silva, D. R. Austin, A. Thai, M. Baudisch, M. Hemmer, D. Faccio, A. Couairon, and J. Biegert, "Multi-octave supercontinuum generation from mid-infrared filamentation in a bulk crystal," Nat. Comm. **3**, 807 (2012).
8. P. B. Petersen and A. Tokmakoff, "Source for ultrafast continuum infrared and terahertz radiation," Opt. Lett. **35**(12), 1962–1964 (2010).
9. M. D. Thomson, V. Blank, and H. G. Roskos, "Terahertz white-light pulses from an air plasma photo-induced by incommensurate two-color optical fields," Opt. Express **18**(22), 23173–23182 (2010).
10. H. Suchowski, D. Oron, A. Arie, and Y. Silberberg, "Geometrical representation of sum frequency generation and adiabatic frequency conversion," Phys. Rev. A **78**(6), 063821 (2008).
11. H. Suchowski, V. Prabhudesai, D. Oron, A. Arie, and Y. Silberberg, "Robust adiabatic sum frequency conversion," Opt. Express **17**(15), 12731–12740 (2009).
12. H. Suchowski, B. D. Bruner, A. Ganany-Padowicz, I. Juwiler, A. Arie, and Y. Silberberg, "Adiabatic frequency conversion of ultrafast pulses," Appl. Phys. B **105**(4), 697–702 (2011).
13. J. Moses, H. Suchowski, and F. X. Kärtner, "Fully efficient adiabatic frequency conversion of broadband Ti:sapphire oscillator pulses," Opt. Lett. **37**(9), 1589–1591 (2012).
14. C. Heese, C. R. Phillips, B. W. Mayer, L. Gallmann, M. M. Fejer, and U. Keller, "75 MW few-cycle mid-infrared pulses from a collinear apodized APPLN-based OPCPA," Opt. Express **20**(24), 26888–26894 (2012).

#197778 - $15.00 USD Received 17 Sep 2013; revised 25 Oct 2013; accepted 27 Oct 2013; published 15 Nov 2013

15. C. R. Phillips and M. M. Fejer, "Adiabatic optical parametric oscillators: steady-state and dynamical behavior," Opt. Express **20**(3), 2466–2482 (2012).
16. G. Porat and A. Arie, "Efficient, broadband, and robust frequency conversion by fully nonlinear adiabatic three-wave mixing," J. Opt. Soc. Am. B **30**(5), 1342–1351 (2013).
17. C. R. Phillips, C. Langrock, D. Chang, Y. W. Lin, L. Gallmann, and M. M. Fejer, "Apodization of chirped quasi-phasematching devices," J. Opt. Soc. Am. B **30**(6), 1551–1568 (2013).
18. B. Mayer, C. Phillips, L. Gallmann, M. Fejer, and U. Keller, "Sub-4-cycle laser pulses directly from a high-repetition-rate, mid-infrared OPCPA at 3.4 μm," Opt. Lett. (to be published).
19. N. Baranova, "Adiabatic transition of the pump into second optical harmonic," Sov. Phys. JETP Lett. **57**, 790–793 (1993).
20. L. D. Landau, "Theorie der energieubertragung. II," Phys. Sov. Union **2**, 46–51 (1932).
21. C. Zener, "Non-adiabatic crossing of energy levels," Proc. R. Soc. Lond., A Contain. Pap. Math. Phys. Character **137**(833), 696–702 (1932).
22. O. Gayer, Z. Sacks, E. Galun, and A. Arie, "Temperature and wavelength dependent refractive index equations for MgO-doped congruent and stoichiometric LiNbO3," Appl. Phys. B **91**(2), 343–348 (2008).
23. I. Shoji, T. Kondo, A. Kitamoto, M. Shirane, and R. Ito, "Absolute scale of second-order nonlinear-optical coefficients," J. Opt. Soc. Am. B **14**(9), 2268–2294 (1997).
24. J. Moses, S.-W. Huang, K.-H. Hong, O. D. Mücke, E. L. Falcão-Filho, A. Benedick, F. Ö. Ilday, A. Dergachev, J. A. Bolger, B. J. Eggleton, and F. X. Kärtner, "Highly stable ultrabroadband mid-IR optical parametric chirped-pulse amplifier optimized for superfluorescence suppression," Opt. Lett. **34**(11), 1639–1641 (2009).
25. T. Fuji, N. Ishii, C. Y. Teisset, X. Gu, T. Metzger, A. Baltuska, N. Forget, D. Kaplan, A. Galvanauskas, and F. Krausz, "Parametric amplification of few-cycle carrier-envelope phase-stable pulses at 2.1 microm," Opt. Lett. **31**(8), 1103–1105 (2006).

1. Introduction

The fields of nonlinear infrared spectroscopy [1] and strong-field laser-matter interaction science [2] demand broadband, coherent, energetic sources of mid-IR light. Currently, such broadband amplifiers covering the 2-6 μm spectral range are lacking. Success has been achieved to some degree by several candidate technologies, including optical parametric amplifiers and doubly resonant optical parametric oscillators [3, 4], conventional difference frequency generation [5, 6], and plasma-filament self-compression or optical rectification driven by mid-IR or UV/VIS light pulses [7–9]. As of yet, each of these technologies for producing broadband mid-IR light is currently insufficient in some respect for producing multi-octave spanning, energetic (μJ to mJ) sources with relatively flat spectral power distribution.

Here we present the proof of principle of a new approach for the efficient conversion of broadband near-IR sources to ultrabroad (greater than octave spanning) mid-IR bands, applicable for external frequency conversion for many near-IR laser systems. With the addition of an adiabatic frequency converter (consisting of only a single nonlinearly and adiabatically chirped quasi-phase-matching grating in magnesium oxide doped lithium niobate) to the output of a near-IR broadband optical parametric chirped pulse amplifier (OPCPA), we demonstrate efficient downconversion of the near-IR pulse to a 1.1-octave mid-IR band spanning 2-5 μm with 1.5-μJ energy. The experiment proves the scalability of the adiabatic frequency conversion method to an extreme bandwidth. Moreover, we demonstrate the ability to shape the mid-IR power spectrum by use of a pulse shaper in the near-IR laser.

The concept of adiabatic frequency conversion, introduced only recently, utilizes an analogy between coherently excited two-level quantum systems and electromagnetic waves coupled by an undepleted pump wave in a nonlinear crystal with an aperiodically poled quadratic susceptibility tensor [10, 11]. It has resolved the bandwidth-efficiency trade-off, and achieved efficient scalable broadband frequency conversion. The method was first experimentally realized for sum frequency generation (SFG) from the near-IR into the visible, and facilitated broad bandwidth conversion with very high efficiency [10]. It was confirmed that the conversion process is insensitive to small changes in parameters that affect the phase mismatch such as crystal temperature, interaction length, angle of incidence, and input wavelength [11]. The concept was applied successfully to the upconversion and downconversion of ultrashort pulses, applying the mechanism of 'chirp pulse conversion' (i.e.

#197778 - $15.00 USD Received 17 Sep 2013; revised 25 Oct 2013; accepted 27 Oct 2013; published 15 Nov 2013

stretching the ultrashort seed pulse prior to the conversion process), where conversion of Ti:S oscillator pulses with near-100% efficiency for a broadband spectrum has been obtained [12, 13]. Also, the Landau-Zener theory for adiabatic passage was experimentally verified, showing that in the adiabatic limit, the conversion efficiency asymptotically approaches unity with no frequency back-conversion for a broad spectral range [13]. Later, it was shown that the adiabatic evolution can be applied for efficient conversion of ultrashort pulses in optical parametric amplifier and oscillator systems [14, 15]. In recent research done independently by two groups, the analysis of adiabatic evolution in the fully nonlinear three-wave-mixing regime was theoretically analyzed [16, 17], showing a greater energy scalability, which is especially important for efficient OPA applications (a topic that has been probed recently by other groups [14, 18]).”

This article is organized as follows. In section 2, we briefly detail the adiabatic difference frequency conversion concept and discuss the design of an octave-spanning adiabatic frequency converter device. In section 3, we outline the experimental apparatus. In section 4, we present our experimental results of near full photon number conversion of an 8-μJ OPCPA pulse spanning 680-870 nm which is mixed with a narrowband 1047-nm pulse, generating an octave spanning mid-IR spectrum from 2.1 to 4.7 μm at −10 dB of peak. Section 5 is devoted to the conclusion and future outlook.

2. Adiabatic difference frequency conversion – design and numerical prediction

The design of an adiabatic frequency converter is based on adiabatic evolution and the Landau-Zener (LZ) theorem, presented in detail in previous works [10–12, 19]. The LZ theorem [20, 21], which provides valuable insight into the adiabatic dynamics, was originally applied to spin-½ systems, photo-dissociation of molecules, quantum control of atomic systems, and recently for efficient and robust frequency conversion [20, 21]. The theorem can estimate the probability of electron transitions in two-level systems while providing a measurement of the adiabaticity, or more accurately the amount of diabaticity (non-adiabatic corrections) of the interaction. It is extremely valuable for describing adiabatic frequency conversion in SFG/DFG processes where the pump photon number greatly exceeds the signal and idler photon numbers, as the frequency conversion dynamics under the undepleted pump approximation are perfectly analogous to the quantum dynamics. The expression for the signal-to-idler conversion efficiency of the SFG/DFG processes is given by [12]:

$$\eta_{LZ}\left(z\to\infty\right)=1-e^{-\frac{2\pi|\kappa|^2}{|d\Delta k/dz|}}, \tag{1}$$

where $\kappa^2=2.232d_{eff}^2 I_2/n_1n_2n_3\lambda_1\lambda_3 c$, and d_{eff} is the effective second-order susceptibility in pm/V; I_2 is the pump intensity in MW/cm^2; n_1, n_2, n_3, are signal, pump, and idler indices of refraction; λ_1 and λ_3 are signal and idler wavelengths in cm; $c=2.998\times10^{10}$ cm/s; and the sweep rate $\left|d\Delta k/dz\right|$ is in cm^{-2}.As seen, the exponent has a linear dependence on I_2 and on d_{eff}^2, and is inversely proportional to $\left|d\Delta k/dz\right|$. The efficiency depends exponentially on an adiabatic parameter, defined as $\alpha\equiv\frac{|d\Delta k/dz|}{2\pi|\kappa|^2}$, *i.e.*, the ratio between the sweep rate of the phase mismatch, $d\Delta k/dz$, and the square of the coupling coefficient, κ^2. *Adiabatic propagation* is obtained when $\alpha\ll1$, which is the asymptotic case corresponding to unity conversion efficiency. This can be achieved either by changing the sweep rate slowly at a given pump intensity, or by applying a strong pump for a given sweep rate. A nice comparison of the three different dynamical regimes, $\alpha\gg1,\alpha\sim1$, and $\alpha\ll1$ (diabatic, semi-diabatic and adiabatic trajectories), can be further viewed in [11].

#197778 - $15.00 USD Received 17 Sep 2013; revised 25 Oct 2013; accepted 27 Oct 2013; published 15 Nov 2013

In principle, a single adiabatic frequency converter can cover all of the wavelengths that can meet perfect phase matching during propagation along the aperiodically poled nonlinear crystal. For a given crystal design, the available bandwidth is determined proportionally by the length of the nonlinear crystal and inversely by the adiabatic characteristic length, defined as $L_{adiabatic} = \frac{\kappa}{|d\Delta k / dz|}$, which describes the length required for an adiabatic transition between a given set of frequencies [14]. The parameter has a linear relation to the coupling coefficient term (i.e., the pump field amplitude and effective nonlinear susceptibility), and is inversely proportional to the sweep rate $|d\Delta k / dz|$. Thus, both the adiabatic characteristic length and the total length of the crystal are scalable by a proper design. In practice, the bandwidth is limited by the maximum crystal length that can be manufactured and by the laser intensity damage threshold. It is also worth noting that the region along the nonlinear crystal where each IR spectral component is generated is the region where the local QPM pitch compensates the material phase-mismatch. Before and after this region, the QPM pattern does not eliminate the large phase mismatch, resulting in minimal backconversion and cascading processes. This allows robust efficient conversion for various intensities, as in a Gaussian beam profile. In the work reported here, we find that a crystal length of 2 cm is already long enough for a conversion bandwidth greater than an octave. Note, a precise definition of the bandwidth of adiabatic frequency conversion processes, even for the depleted nonlinear case (i.e., without assuming an undepleted pump) is detailed in [16].

Using the quasi-phase matching (QPM) technique, we have designed an adiabatic aperiodically poled grating in a magnesium-oxide-doped congruent lithium niobate (MgCLN) nonlinear crystal. The poling satisfies the constraints imposed by the adiabatic inequality and the LZ prediction of Eq. (1) for a signal range of 600 to 870 nm, mixed with a 1047-nm strong narrowband pump, producing an idler range of 1405 to 5500 nm. We chose to use MgCLN nonlinear crystal for its wide spectral transparency window and high damage threshold. In our simulation, we have used the Sellmeier coefficients retrieved from [22]. Although those coefficients were examined only up to wavelength of 4 μm, we have used them to calculate the adiabatic evolution even for higher wavelengths, exceeding 5 μm. In order to induce an adiabatic longitudinal change of the effective total phase mismatch parameter, defined as $\Delta k(z) = k_2 + k_3 - k_1 - G(z)$, we chose the function $G(z) = 990z^2 + 2400z + 4050$ [1/cm], where z (in cm) is measured from the center of the crystal (i.e., z varied from -1 cm to 1 cm). This design optimized, across signal frequencies, the uniformity of the adiabatic conversion rate, and has a QPM period, $\Lambda(z) = 2\pi / G(z)$, ranging from 8.4 to 23.8 μm.

Numerical finite-difference simulations of the design for a pump intensity of 8.1 GW/cm^2 (when assuming an average effective second order susceptibility of $d_{33}(\lambda)$ = 21.5 pm/V – a modified value for a DFG process using a Miller's rule prediction for MgCLN [23]), are shown in Fig. 1. The two-dimensional image shows the conversion efficiency as a function of the propagation length (x-axis) and for a broad output wavelength span covering 1100 nm to 6400 nm (y-axis). In order to better perceive the information, we have plotted in the upper figure several horizontal cross sections of different wavelengths (1500, 2000, 2500, 3000, 4250, 5500 and 6400 nm), showing the adiabatic evolution of those waves. As seen, each signal is adiabatically converted at a different location in the nonlinear crystal.

As can be seen, at the output facet of the nonlinear crystal the predicted photon number conversion efficiency is very high (above 80% for $I_2 >$ 8.1 GW/cm^2 for an idler range of 1.4 to 5.5 μm). These values are in very good agreement with the use of the Landau-Zener formula. Note, these simulations neglect the linear absorption of MgCLN, which can be expected to result in a significant reduction in efficiency above 5-μm wavelength. It is also

#197778 - $15.00 USD Received 17 Sep 2013; revised 25 Oct 2013; accepted 27 Oct 2013; published 15 Nov 2013

worth noting that due to lack of literature data on MgCLN for those long wavelengths, we assume in our numerical simulations that the nonlinear susceptibility is constant for the entire spectral range.

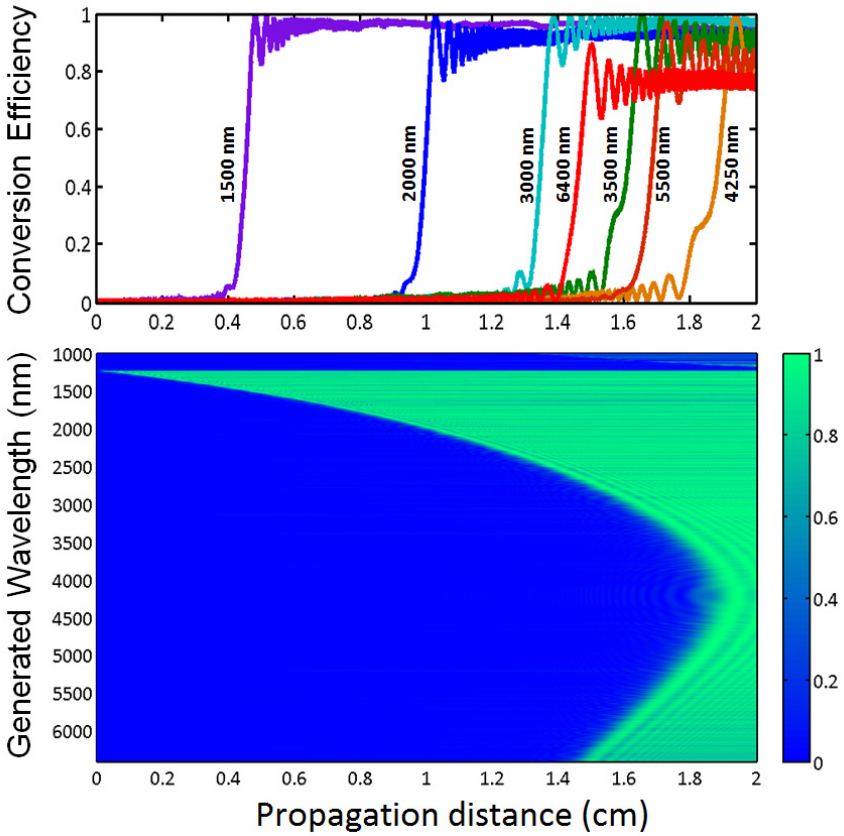

Fig. 1. The octave-spanning adiabatic difference frequency design. Main figure: two-dimensional map of the conversion efficiency as a function of generated wavelength (y-axis) and the location along the adiabatic aperiodically poled nonlinear crystal (x-axis). The pump intensity is 8.1 GW/cm^2. The upper panel shows the conversion efficiency for several wavelengths along the propagation axis. As seen, all are designed to have adiabatic trajectories for efficient conversion from near IR to mid IR. At the output facet of the nonlinear crystal (L = 2 cm), high conversion efficiency is achieved for the 1300-5500 nm spectral range. The details of the design are explained in the main text.

3. Experimental apparatus

Our experimental system was designed to demonstrate the first proof of principle of a mid-IR post amplification converter using adiabatic frequency conversion that may be applied for many other near-IR systems. It consisted of a combination of a near-IR OPCPA and an adiabatic difference frequency generation (ADFG) stage, illustrated in Fig. 2. A Ti:sapphire oscillator injection seeds a Nd:YLF chirped pulse amplifier (CPA), and a 2-stage parametric amplifier. The Nd:YLF CPA is home-built and delivers 12-ps, 1-kHz, 4-mJ pulses at 1047nm [24], which are then used to pump the OPCPA after second harmonic generation (SHG) in a 10-mm-long noncritically phase-matched LBO crystal, and to pump the ADFG process. The near-IR signal pulse source is a modified OPCPA system that delivers 1-kHz, ~4 ps chirped pulses spanning 0.7-0.9 μm with up to 20-μJ energy. In the experiment, these pulses were combined collinearly at a dichroic mirror (DM) with up to ~0.5 mJ of the remaining Nd:YLF

#197778 - $15.00 USD Received 17 Sep 2013; revised 25 Oct 2013; accepted 27 Oct 2013; published 15 Nov 2013

pulse energy at 1047 nm and sent to the aperiodically poled MgCLN grating described in Section 2 for broadband ADFG, with telescopes employed to keep the chirped broadband near-IR beam (*i.e.*, the ADFG "signal") smaller than one-half the size of the 1047-nm beam (*i.e.*, the ADFG "pump"). The MgCLN grating has an aperture of 1 mm x 3 mm.

The OPCPA (Fig. 2, bottom) is capable of delivering 30-μJ, 8-fs, 1-kHz pulses with a bandwidth covering 0.69-1.05μm, and was modified for this application by diverting the amplified beam before the glass compressor normally used to dechirp the pulses, and by narrowing the gain bandwidth to match the 0.69-0.87 μm range desired for later adiabatic conversion. The modified configuration uses 1 or 2 noncollinear optical parametric amplifier (NOPA) stages in BBO, and a combination of grism pairs, dispersive glass, and an acousto-optic programmable dispersive filter (Dazzler, Fastlite) to control the dispersion throughout the experiment. The first NOPA stage consists of a 5-mm thick BBO crystal cut at $\theta = 24.0°$ with a noncollinear angle $\alpha = 2.4°$, pumped by 500-μJ pulses at 523 nm, an energy optimized for a gain of ~10^5 to amplify the weak Ti:sapphire oscillator pulses to ~1-μJ. These are then further amplified in another NOPA, which consists of a 3-mm thick BBO, again with $\theta = 24.0°$, $\alpha = 2.4°$, pumped by 600-μJ pulses at 523nm, resulting in a gain of ~10^3 which compensates for the losses in the dispersive elements between stages, and gives the final output energy of 20 μJ with a clean spatial profile.

Careful considerations were made in regards to the chirp in the NOPA system to ensure that there is a good temporal overlap between the pump and seed in both the NOPA stages and in the ADFG process. The Ti:sapphire seed pulses were first stretched to 2.5 ps in a grism pair with a group velocity dispersion (GVD) of −6300 fs^2, optimized to overlap with the 8-ps NOPA pump pulses for efficient amplification in the 0.69-0.87-μm range in the first NOPA stage. The pulses were then further stretched by a grism + Dazzler combination providing an additional −4000 fs^2 of GVD to stretch the pulse to 3.7 ps. Conveniently, this duration (3.7 ps) was also appropriate for the ADFG stage, allowing good overlap with the 12-ps pump duration. Additionally, the 3.7-ps duration was long enough to prevent significant group velocity walkoff between the interacting pulses and compression of the signal pulses due to the normal dispersion of MgCLN at near-IR wavelengths.

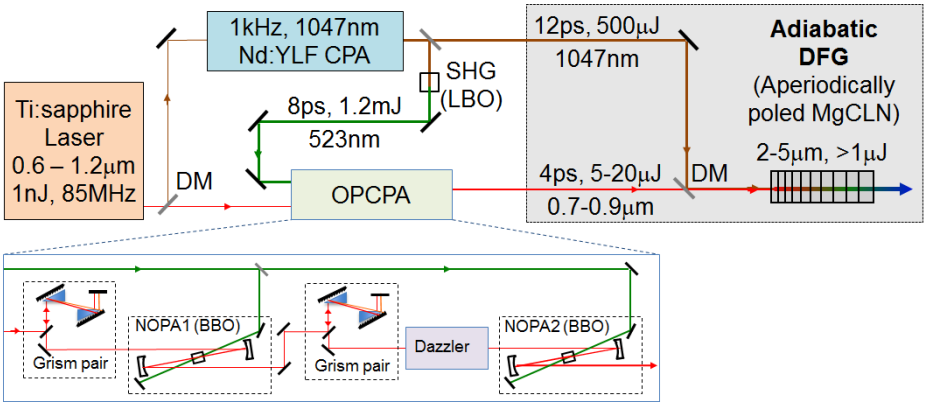

Fig. 2. Experimental setup for adiabatic difference frequency conversion of OPCPA pulses (top) and detail of the OPCPA system (bottom). Further details can be found in the main text.

The mid-IR power was collected by a scanning monochromator with a thermo-electrically cooled PbSe photodetector (Horiba/JY). The relative spectral intensity response of the monochromator and photodetector were calibrated with a temperature-controlled black-body source. A Ge order-sorting filter was used to block any residual NIR leakage.

#197778 - $15.00 USD Received 17 Sep 2013; revised 25 Oct 2013; accepted 27 Oct 2013; published 15 Nov 2013

4. Experimental results

The experimental validation of the octave-spanning downconversion consists of several sets of experiments. By using various broadband OPCPA input pulses with variable spectral profiles, we could verify the response of the conversion device and demonstrate its applicability for accurate conversion of broadband near-IR pulses.

Figure 3 shows the normalized measured power spectrum (solid curve) of a generated mid-IR pulse alongside the normalized "expected" power spectral density (dashed black curve) calculated by assuming 100% conversion of the OPCPA power spectrum to the mid-IR via ADFG and accounting for the varying quantum defect, $\lambda_{signal}/\lambda_{idler}$. We observe a clear transfer of the spectral amplitude profile from near-IR to mid-IR, resulting in observable power spectral density on a linear scale from 2 to 5 μm. At −10 dB of peak, the spectrum spans 2.1-4.7 μm, or 1.1 octaves = $\log_2[4.7\mu m / 2.1\mu m]$. The maximum mid-IR pulse energy we obtained is 1.5 μJ, equivalent to an 83% internal photon number conversion of the 7.9 μJ of OPCPA pulse energy in the incident 680-870-nm range (see inset), once we have accounted for the 23% quantum efficiency integrated over the spectrum. This is slightly lower than the expected ~90% internal photon number conversion efficiency expected from our simulations. The small discrepancies between expected and measured power spectra are under current investigation, and are likely due to ambient absorption, QPM grating manufacturing errors, and/or linear absorption in the MgCLN crystal at long wavelengths. We note that we observed by eye a small amount of green and violet light emanating from the lithium niobate grating, indicating some parasitic second harmonic generation of the pump and signal waves. The pump loss appeared negligibly small, but the signal loss could account for the few-percent discrepancy between expected and measured mid-IR power. Generally, these processes are not directly phase-matched by first-order QPM in our design, so do we not expect them to be limiting, but this could plausibly be a limitation for designs requiring a significantly higher pump or signal intensity.

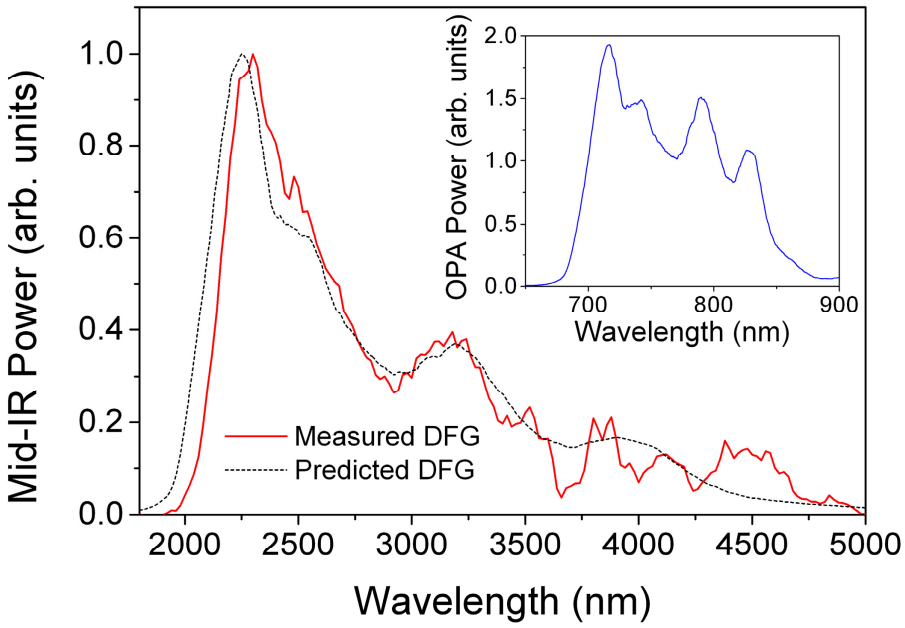

Fig. 3. Octave-spanning mid-IR spectrum. The red solid curve is the experimental spectrum, while the dashed black line is the normalized expected spectrum, assuming a100% photon number conversion efficiency. Inset: the inputted near-IR spectrum from the OPCPA.

#197778 - $15.00 USD Received 17 Sep 2013; revised 25 Oct 2013; accepted 27 Oct 2013; published 15 Nov 2013

The mid-IR beam was imaged using a pyroelectric array imager, and displayed a nearly Gaussian profile with an ellipticity of 1.2, comparable to the ellipticity of the input near-IR beam, which had an ellipticity of 1.1. We note that the ellipticity of the mid-IR beam depended critically on the alignment, increasing as we misaligned the system by introducing a non-collinear angle between the pump and signal beams. To test the frequency dependence of the mid-IR beam profile, we used the AOPDF to select portions of the input near-IR spectrum spanning roughly one-third of the full spectral width. The resulting portions of the mid-IR spectrum after conversion showed no significant variation in beam size, shape or location.

In order to further examine the adiabatic difference frequency converter, we have measured not only the generated signal in the mid-IR regime, but also the depletion of the incoming near-IR OPCPA pulses, and from this we have analyzed the implied conversion efficiency. The measured near-IR spectral power densities can be seen explicitly in the inset of Fig. 4, where black, red and green curves are for pump intensities of 0 GW/cm^2, 5.2 GW/cm^2, and 13.2 GW/cm^2, respectively. To calculate the implied conversion efficiency for each spectral component, we have used the following relation:

$$\eta(\lambda) = \frac{P_0(\lambda) - P_{I_p}(\lambda)}{P_0(\lambda)}, \tag{2}$$

Where P_{Ip} is the spectral power density for a specific pump power I_p, and P_0 is the undepleted near-IR spectrum (where the narrowband pump was not used, and thus, I_p = 0). Figure 4 shows the resulting implied conversion efficiencies obtained from the near-IR spectral depletion and Eq. (2) (solid red and black curves for the two pump intensities, respectively), alongside the simulated conversion efficiency as a function of the input wavelengths for two pump intensities, 3.2 GW/cm^2 and 8.1 GW/cm^2 (dashed blue and gray curves for the two pump intensities, respectively). As seen, though the simulated pump intensity values differ from each of the respective experimental values by a factor of 1.6, the numerical predictions of the conversion efficiency for both of the pump intensities are in very good agreement with the retrieved conversion efficiency. This is true for spectral components of the near-IR field as high as 870 nm (which corresponds to 5500 nm in the mid IR). Also, the good agreement of the conversion efficiency between 4000 and 6000 nm expands the literature values for MgCLN nonlinear crystal beyond the reported values examined in [22]. The factor of 1.6 can be explained partially by the fact that the average experimental pump intensity overlapped with the near-IR pulse is lower than the corresponding peak intensity. It might also be explained by the fact that in our numerical simulations, we have assumed an average nonlinear susceptibility of $d_{33}(\lambda) =$ 21.5 pm/V for the entire spectral range, which is an estimated average value of the effective nonlinear susceptibility using the Miller's rule prediction for the DFG process. In the mid-IR, this value varies from $d_{33}\left(\lambda_s = 690\,\text{nm}, \omega_p = 1047\,\text{nm}; \omega_i = 2025\,\text{nm}\right) \approx 24\,\text{pm/V}$ to $d_{33}\left(\lambda_s = 900\,\text{nm}, \omega_p = 1047\,\text{nm}; \omega_i = 6400\,\text{nm}\right) \approx 19\,\text{pm/V}$, where we took Miller's delta to be $\Delta_{miller} = 16\,\text{pm/V}$. The true value might be even lower, due to the fact that the experimental verification of the 2nd-order susceptibility has been shown to have a deviation from Miller's rule [23]. As shown before, the coupling coefficient between the interacting waves is proportional to $\kappa \propto d_{eff}^2 I_2$, meaning that an inaccurate value of d_{33} will have a strong impact. Note, the data presented in Fig. 4 also confirms the insensitivity of the adiabatic conversion rate to the signal intensity, as we see a flat conversion efficiency over a wavelength range including near-IR power spectral densities as low as −10dB relative to the peak.

#197778 - $15.00 USD Received 17 Sep 2013; revised 25 Oct 2013; accepted 27 Oct 2013; published 15 Nov 2013

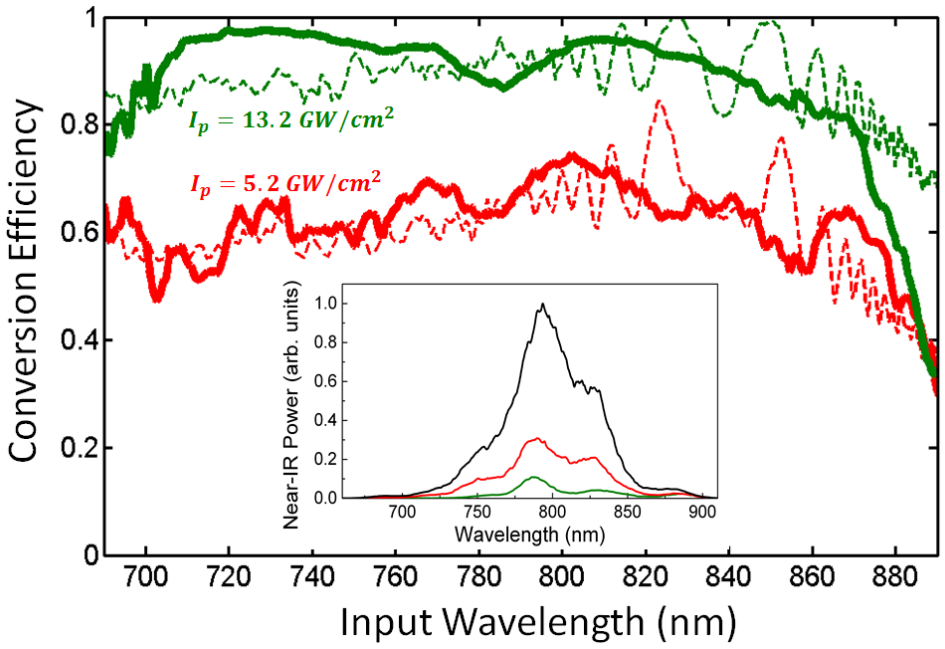

Fig. 4. Conversion efficiency (solid curves), following Eq. (2), retrieved from the experimentally observed depletion of the near-IR power spectra as a function of pump intensity .The simulated conversion efficiencies at the output facet of the nonlinear crystal are also plotted (dashed lines), using values of the pump intensity a factor of 1.6 lower than the two experimental values, respectively. The measured near-IR spectral power densities are shown explicitly in the inset, where black, red and green curves are for pump intensities of 0, 5.2 and 13.2 GW/cm^2, respectively. The numerical predictions and the measured conversion efficiencies are in very good agreement for spectral components as high as 870 nm (which corresponds to 5500 nm).

In the last set of experiments, we have further examined the expected flatness of the conversion response. With the Dazzler acoustic pulse shaper that we have in the OPCPA apparatus (see Fig. 2), spectral holes were created in the near-IR spectral power densities. These can be seen in Fig. 5(a). The black, green, blue and red curves correspond to near-IR spectra with spectral holes inserted at 760 nm, 777 nm, 805 nm and 829 nm. These spectra were efficiently converted to the mid IR, producing spectral power densities with the exact hole locations expected in the mid-IR at 2750 nm, 3000 nm, 3500 nm and 4000 nm (Fig. 5(b)). This good correspondence between spectral profiles provides another verification of the main advantage of the adiabatic frequency conversion method, which is the separation between the seed spectral shape and the flat response of the nonlinear crystal, allowing the robust transfer of the spectral amplitude to another spectral range.

In the experimental results, a ripple can be seen in the power spectra that may possibly be due to the effect of the spectral ripples of the converted device. Those are very significantly seen in the numerical simulation, but averaged out in the experimental retrieval (due to pump intensity averaging in the Gaussian beam). It was shown how apodization (meaning, reducing spectral ripples) can be used to reduce ripple oscillations across the conversion bandwidth [17]. The apodization procedure may be applied to the constant-chirp QPM modulation used in our design to yield a smoother spectral phase.

#197778 - $15.00 USD Received 17 Sep 2013; revised 25 Oct 2013; accepted 27 Oct 2013; published 15 Nov 2013

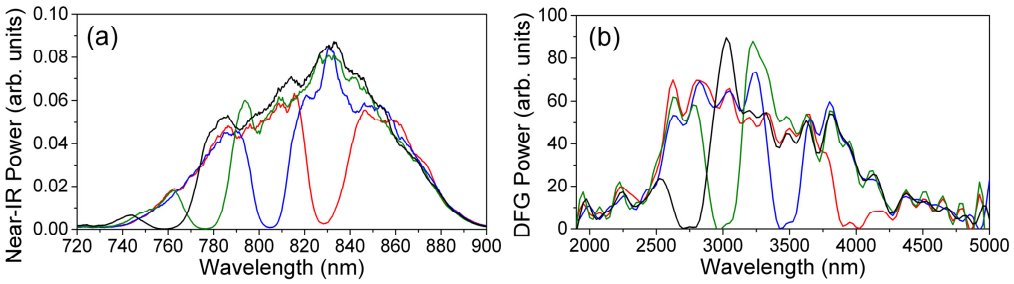

Fig. 5. Efficient and robust conversion of amplitude-shaped spectra. (a) Various OPCPA near-IR pulses that were shaped by a Dazzler in order to eliminate certain wavelength components in their spectral power densities. (b) The converted mid-IR spectra. As seen, one-to-one correspondence of the spectral hole locations and widths is achieved for all spectra.

5. Conclusion

In conclusion, we have demonstrated an octave-spanning mid-IR source at the μJ energy level by adiabatic frequency conversion of near-IR OPCPA pulses, in a scheme we expect will have broad applicability as a post-amplification method for near-IR to mid-IR conversion, potentially allowing single-cycle pulsed sources. It is the beauty of the adiabatic approach to allow, in a single grating, the simultaneous conversion of all frequencies that can be quasi-phase-matched in a given medium (for a given choice of signal, pump, and idler polarizations), as long as a grating with wide enough poling period variation can be manufactured. It is immediately suited for the seeding of a degenerate OPCPA with a narrowband 1-μm pump and chirped 2-μm signal, such as the amplifiers in [24,25]. The amplified pulses can be subsequently compressed to provide a high-energy, few-cycle source suitable, e.g., for strong-field physics. The energy of 1.5 μJ obtained in this work may be further scaled by increasing the input near-IR energy, though intensity damage and B-integral will eventually limit the scaling for a given MgCLN aperture dimension. We are currently investigating the energy limitations of the device. We note, while full conversion efficiency in the difference frequency application presented here does not involve the general three wave type dynamics, where the pump and signal are comparable in intensity (depleted pump regime), this regime would offer greater energy scalability when the pump intensity is limited, and is especially important for efficient OPA applications, a topic that has been probed recently by other groups [12–15].

The next step is to compress such a pulse to its transform-limited duration, which will allow the generation of the first single-cycle mid-IR pulse. The first task is to characterize the spectral phase and confirm that the converted idler possesses a transfer of the signal pulse's spectral phase plus the linear phase accumulated during propagation in the nonlinear crystal [12]. Then a suitable choice of dispersive elements can be employed to dechirp the pulse. We note, because of the expected transfer of signal phase to the idler, the AOPDF included within the near-IR OPCPA could be used to fine-tune the dispersion of the idler pulse, including GVD and higher orders. Using the scalability of the design, the adiabatic DFG technique could potentially be used to generate multiple-octave-spanning spectra (i.e., having bandwidths that contain wavelengths and their harmonics), allowing the generation of the shortest pulse mid-IR source possible.

Acknowledgements

This work was supported by the United States Air Force Office of Scientific Research (AFOSR) through grants FA9550-12-1-0080 and FA9550-13-1-0159, and by the Center for Free-Electron Laser Science. P.K. acknowledges support by a NDSEG Graduate Fellowship.

#197778 - $15.00 USD Received 17 Sep 2013; revised 25 Oct 2013; accepted 27 Oct 2013; published 15 Nov 2013